CHEMISTRY OF MATERIALS

Article

pubs.acs.org/cm

In Situ Thermal Synthesis of Inlaid Ultrathin MoS_2/Graphene Nanosheets as Electrocatalysts for the Hydrogen Evolution Reaction

Lianbo Ma,[†] Yi Hu,[†] Guoyin Zhu,[†] Renpeng Chen,[†] Tao Chen,[†] Hongling Lu,[†] Yanrong Wang,[†] Jia Liang,[†] Haixia Liu,[†] Changzeng Yan,[†] Zuoxiu Tie,[†] Zhong Jin,*[,†] and Jie Liu*[,†,‡]

[†]Key Laboratory of Mesoscopic Chemistry of MOE and Collaborative Innovation Center of Chemistry for Life Sciences, School of Chemistry and Chemical Engineering, Nanjing University, Nanjing, Jiangsu 210093, China

[‡]Department of Chemistry, Duke University, Durham, North Carolina 27708, United States

Supporting Information

ABSTRACT: Herein, we report a unique thermal synthesis method to prepare a novel two-dimensional (2D) hybrid nanostructure consisting of ultrathin and tiny-sized molybdenum disulfide nanoplatelets homogeneously inlaid in graphene sheets (MoS_2/G) with excellent electrocatalytic performance for HER. In this process, molybdenum oleate served as the source of both molybdenum and carbon, while crystalline sodium sulfate (Na_2SO_4) served as both reaction template and sulfur source. The remarkable integration of MoS_2 and graphene in a well-assembled 2D hybrid architecture provided large electrochemically active surface area and a huge number of active sites and also exhibited extraordinary collective properties for electron transport and H^+ trapping. The MoS_2/G inlaid nanosheets deliver ultrahigh catalytic activity toward HER among the existing electrocatalysts with similar compositions, presenting a low onset overpotential approaching 30 mV, a current density of 10 mA/cm^2 at ~110 mV, and a Tafel slope as small as 67.4 mV/dec. Moreover, the strong bonding between MoS_2 nanoplatelets and graphene enabled outstanding long-term electrochemical stability and structural integrity, exhibiting almost 100% activity retention after 1000 cycles and ~97% after 100 000 s of continuous testing (under static overpotential of −0.15 V). The synthetic strategy is simple, inexpensive, and scalable for large-scale production and also can be extended to diverse inlaid 2D nanoarchitectures with great potential for many other applications.

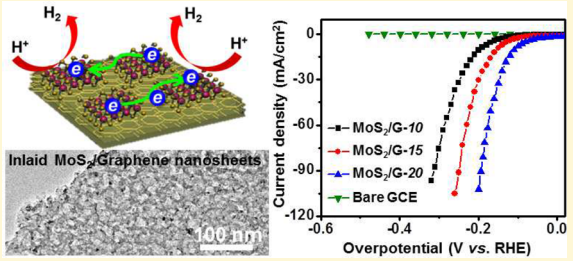

INTRODUCTION

To meet the rapidly growing energy and environmental demands, various approaches have been developed to exploit renewable and clean energy for replacing traditional fossil fuels.[1−4] Hydrogen, as a remarkable energy carrier, has held tremendous promise for sustainable green energy innovation due to its high energy storage capability and pollution-free characteristic.[5,6] Recently, hydrogen production by electrochemical water splitting has caught great attention because of the high efficiency and eco-friendliness.[7,8] However, due to the intrinsically slow kinetics of hydrogen evolution reaction (HER), it is necessary to modify the cathodes with active catalysts.[9,10] Platinum (Pt)-group metals are the most effective electrocatalysts for HER,[11,12] but the scarcity and high cost severely restricted their practical applications.[13] Thus, intensive effort has been devoted to designing and fabricating noble metal-free electrocatalysts for HER.

Currently, noble-metal-free electrocatalysts includeing transition metal chalcogenides,[14−16] phosphides,[17−21] nitrides,[22−25] and carbides[26−29] have emerged as new candidates for HER. Molybdenum disulfide (MoS_2), the two-dimensional (2D) sheet of vertically stacked S−Mo−S interlayers,[30] has attracted great interest as a potential HER catalyst due to its highly reactive atomic active sites exposed at the edges. Recently, several methods for preparing MoS_2-based electrocatalysts have been developed, such as simple mixing, solution-phase synthesis, or chemical vapor deposition (Table S1). However, the inherent stacking nature among MoS_2 layers seriously limits the amount of exposed active sites.[31] Therefore, it is of great importance to increase the exposed active sites and prevent the stacking and aggregation of MoS_2 layers. Despite the great progress achieved so far, the critical problem of preventing the stacking and reducing the size of MoS_2 sheets still remains unresolved.

Apart from the density and reactivity of active sites, the catalytic performance of electrocatalysts is also influenced by several additional factors, such as the charge and ion transport of the cathode. To circumvent these obstacles, here we propose a unique thermal synthesis approach to prepare a novel 2D hybrid nanostructure consisting of ultrathin MoS_2 nanoplatelets inlaid into graphene sheets (MoS_2/G) by using metal oleate as precursor and salt crystals as template. It is worth emphasizing that this new method involving sequential "coating−annealing−washing" steps, is very unique and different from the exiting

Received: May 16, 2016
Revised: July 19, 2016
Published: July 26, 2016

DOI: 10.1021/acs.chemmater.6b01980
Chem. Mater. 2016, 28, 5733−5742

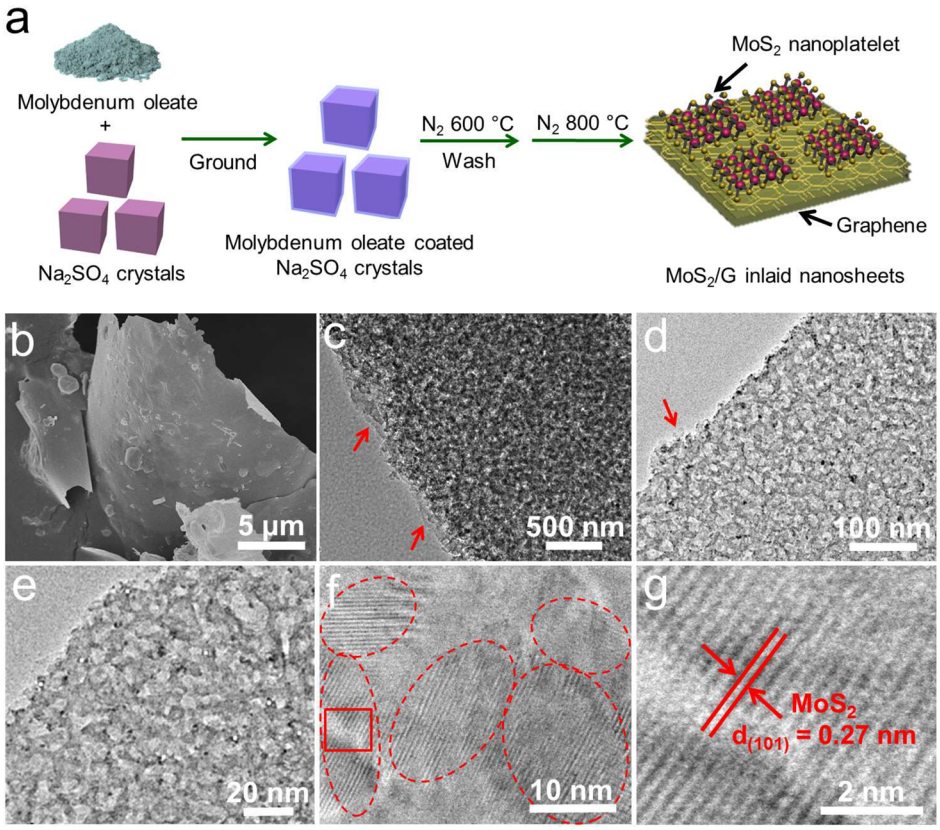

Figure 1. (a) Schematic illustration of the synthesis procedure of MoS_2/G inlaid nanosheets. (b) FESEM, (c–e) TEM, and (f, g) HRTEM images of the MoS_2/G-20 product. The MoS_2/G-20 inlaid nanosheets exhibited a typical 2D planar structure with ultrathin MoS_2 nanoplatelets uniformly implanted in graphene sheets. (g) The magnified view of the rectangle area in (f) and the lattice distance of 0.27 nm corresponds well with the (101) plane of MoS_2, further confirming the synthesis of MoS_2 nanoplatelets.

methods in the literature (Table S1).[32−45] In addition, this method is very facile and suitable for mass production. The resultant ultrathin and tiny-sized MoS_2 nanoplatelets were homogeneously inlaid in the graphene nanosheets, which cannot be achieved by other approaches. The merits of this architecture are that the uniformly distributed small MoS_2 nanoplatelets provide ultrahigh electrochemically active surface area (ECSA) and a huge number of exposed active sites for HER, the graphene sheets greatly promote electron transport and H^+ trapping, and the strong bonding between MoS_2 and graphene ensure high structural stability in electrochemical tests. As a consequence, the synergistic effect of ultrathin MoS_2 nanoplatelets and graphene sheets result in the excellent electrocatalytic performance of MoS_2/G inlaid nanosheets toward HER.

EXPERIMENTAL SECTION

Chemicals. Molybdenum chloride ($MoCl_5$) was purchased from Sigma-Aldrich, and other chemicals were purchased from Sinopharm Chemical Reagent Co., Ltd. All chemicals are of analytical purity and used without further purification.

In Situ Thermal Synthesis of MoS_2/G Inlaid Nanosheets. Typically, 0.80 mmol of $MoCl_5$ was dissolved into 2.0 mL of deionized water. Subsequently, 4.0 mmol of sodium oleate was added into the above solution under vigorous stirring. The resulting mixture was aged at 85 °C for 6 h to obtain molybdenum oleate. Then the mixture was grounded with a specific amount of sodium sulfate (Na_2SO_4) crystals thoroughly. After that, the mixture was put into a tube furnace and heated to 600 °C for 2 h in a N_2 atmosphere with a ramp rate of 2 °C/min. The resultant powder was put into 30 mL of deionized water and stirred for 1 h, then collected by centrifugation, and dried at 80 °C for 12 h in a vacuum oven. In order to obtain the final product, the collected powder was further annealed at 800 °C for 2 h in N_2 atmosphere with the same ramp rate. For the synthesis of MoS_2/G-10, MoS_2/G-15, MoS_2/G-20, and MoS_2/G-25 products, 10, 15, 20, and 25 g of Na_2SO_4 crystals were used, respectively.

Hydrothermal Preparation of MoS_2–Graphene Composite as a Control Sample. First, graphene oxide (GO) was prepared from nature graphite flake by a modified Hummers method.[46] For the synthesis of the MoS_2–graphene composite, 120 mg of sodium dodecyl sulfonate was added into 30 mL of deionized water that containing 30 mg of GO. Then, 100 mg of $Na_2MoO_4{\cdot}2H_2O$ and 200 mg of thiourea (C_2H_5NS) were introduced into the above solution and further stirred for 30 min. After that, the resultant mixture was transferred into an autoclave and heated at 180 °C for 20 h. Finally, the precipitate was collected by centrifugation, washed with absolute ethanol, and dried in a vacuum oven for 12 h.

Characterizations. The morphology, size, and structure of the products were examined by field-emission scanning electron microscopy (FESEM, JSM-6480), transmission electron microscopy (TEM, JEM-2100), and an energy-dispersive X-ray (EDX) spectroscope attached to the field-emission scanning electron microscope. The crystallinities of as-synthesized samples were characterized by powder X-ray diffraction (XRD) on a Bruker D-8 Advance diffractometer using Cu Kα (λ = 1.5406 Å) radiation at a scanning rate of 6°/min. Thermogravimetric analysis (TGA) was performed on a NETZSCH STA 449 C instrument in air atmosphere from room temperature to 800 °C at a heating rate of 10 °C min^{-1}. X-ray photoelectron spectra (XPS) were obtained using a PHI-5000 VersaProbe X-ray photoelectron spectrometer with an Al Kα X-ray radiation. Raman spectra were collected with a Horiba JY H800 Raman spectrometer using a 532 nm laser source. Nitrogen adsorption–desorption isotherms were obtained through Brunauer–

DOI: 10.1021/acs.chemmater.6b01980
Chem. Mater. 2016, 28, 5733−5742

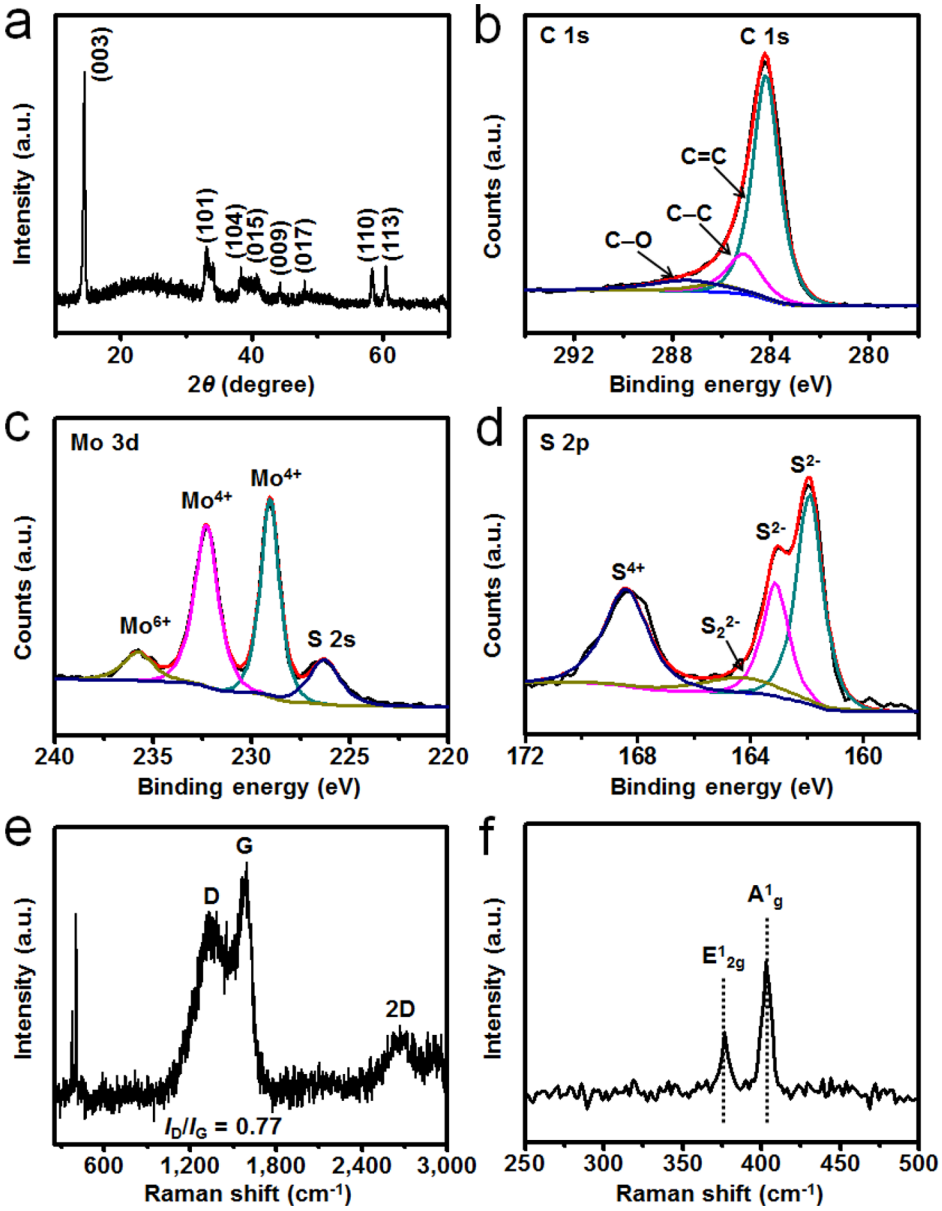

Figure 2. (a) XRD pattern, high-resolution XPS spectrum of (b) C 1s region, (c) Mo 3d region, (d) S 2p region, (e) Raman spectrum, and (f) enlarged Raman spectrum (250−500 cm^{-1}) of the MoS_2/G-20 product.

Emmett−Teller (BET) analysis at 77 K on a Micromeritics ASAP2020 instrument.

Electrochemical Measurements. The catalytic performances of the as-prepared samples toward HER were conducted on a typical three-electrode setup using a CHI 760E electrochemical analyzer (Chenhua Instruments, Shanghai) at room temperature. The electrocatalyst dispersed onto a glassy carbon rotating disk electrode (GCE, ALS Co., Japan) was used as a working electrode, while a calibrated saturated calomel electrode (SCE) and a platinum foil served as the reference and counter electrodes, respectively. The GCE has a diameter of 5.0 mm, and the loading amount of catalyst is 0.25 mg/cm^2. Prior to the surface coating, the GCE was polished by Al_2O_3 powders with size down to 0.05 μm, followed by sonication in absolute ethanol for 10 s, and then allowed to dry at room temperature. To fabricate the working electrode, catalyst ink was prepared by dispersing 5.0 mg of electrocatalyst into a mixed solvent containing 0.98 mL of absolute ethanol and 20 μL of 5.0 wt % Nafion solution, and then the mixture was sonicated for 30 min to form a homogeneous ink. After that, 10 μL of the catalyst ink was loaded onto the polished GCE and dried at room temperature naturally. Linear sweep voltammetry (LSV), cyclic voltammetry (CV), electrochemical impedance spectroscopy (EIS), chronoamperometry measurements, and chronopotentiometric measurements were then conducted, and the LSV was performed at a scan rate of 2.0 mV/s. In this study, the onset overpotential was defined as the potential at a current density of 0.5 mA/cm^2. During the electrochemical measurement, the electrolyte (0.50 M H_2SO_4) was degassed by bubbling high purity nitrogen to eliminate the dissolved oxygen. A gas chromatograph (Agilent GC7890) was employed to analyze the volume of generated H_2 during the electrochemical measurements. The detailed calibration of SCE was provided in Supporting Information. All the potentials reported in our work were calibrated with a reversible hydrogen electrode (RHE) according to the equation $E_{RHE} = E_{SCE} + 0.241$ V.

RESULTS AND DISCUSSION

The typical synthetic procedure for MoS_2/G inlaid nanosheets is depicted in Figure 1a. Molybdenum oleate was grounded with sodium sulfate (Na_2SO_4) crystals to obtain very fine composite powders. In this process, oil-like slimy molybdenum

DOI: 10.1021/acs.chemmater.6b01980
Chem. Mater. 2016, 28, 5733−5742

oleate was uniformly coated on the surface of Na_2SO_4 crystals. Subsequently, the mixture was annealed at 600 °C in a N_2 atmosphere. This led to the decomposition of molybdenum oleate into carbon, molybdenum oxides, etc. (Figure S1a), and thus carbon layers were formed on the surface of the Na_2SO_4 crystals. Subsequently, the surface layer of the Na_2SO_4 crystals was partially reduced by carbon to form Na_2S, and then the facets of Na_2SO_4 also acted as 2D templates to induce the reaction of Na_2S and molybdenum oxides, resulting in the formation of tiny MoS_2 nanoplatelets inlaid carbon layers supported by the remaining Na_2SO_4 crystals (Figure S1b). The detailed reaction processes for explicating the formation of ultrathin MoS_2 nanoplatelets are proposed in eqs S1−4 of the Supporting Information. After removing the residual Na_2SO_4 crystals by washing in excessive water, the collected powder was annealed once again at 800 °C in a N_2 atmosphere to form graphene sheets with further increased graphitic degree. In this way, novel 2D MoS_2/G inlaid nanosheets composed of ultrathin MoS_2 nanoplatelets embedded in graphene sheets were synthesized. We denoted MoS_2/G-x as the final products, where x corresponded to the amount of Na_2SO_4 crystals (x = 10, 15, 20, or 25 g) used in the synthesis process. Of particular note, the starting materials and synthetic process in this work are both viable for large-scale production, making this approach very attractive for practical applications.

Field-emission scanning electron microscopy (FESEM) and transmission electron microscopy (TEM) were employed to investigate the morphology of MoS_2/G inlaid nanosheets. Figure 1b shows a FESEM image of the MoS_2/G-20 product. The inlaid nanosheets exhibit a typical 2D flat structure with rather smooth surface and uniform thickness, and the lateral size exceeds 10 μm. The 2D structure and sheet size were attributed to the flat facets of Na_2SO_4 crystals, which served as the reaction templates. TEM characterizations (Figure 1c−e) confirmed the planar morphology of MoS_2/G-20 with uniformly dispersed inlays. Graphene fringes were found at the edges of nanosheets, as marked with red arrows (Figure 1c,d), and the layer number was closely correlated to the amount of carbonized molybdenum oleate. Tiny nanoplatelets with the size range of 10−20 nm were homogeneously embedded in graphene sheets (Figure 1e), and correspondingly, crystal lattices (as marked by red cycles) were observed in the high-resolution TEM (HRTEM) image (Figure 1f). The lattice spacing of 0.27 nm (Figure 1g) is in accordance with the (101) plane of MoS_2, confirming the synthesis of MoS_2 nanoplatelets. Moreover, to reveal the thickness of MoS_2 in the MoS_2/G-20 product, more HRTEM characterizations were performed. As shown in Figure S2, the observed interlayer distances are 0.74 nm, corresponding to the (002) planes of MoS_2, and the platelet thickness is 3.7 nm, suggesting that the inlaid MoS_2 nanoplatelets are with ultrathin thickness. Compared with the previously reported MoS_2-based materials,[32−45] this architecture can ensure excellent electron transfer between MoS_2 nanoplatelets and graphene sheets, and the uniform dispersion of ultrathin MoS_2 nanoplatelets on graphene sheets can undoubtedly favor the full utilization of exposed active sites, thus contributing to the significantly enhanced catalytic performance toward HER.

The crystalline structure and compositions of MoS_2/G inlaid nanosheets were examined by X-ray diffraction spectroscopy (XRD), energy dispersive X-ray spectroscopy (EDX), and X-ray photoelectron spectroscopy (XPS). As shown in Figure 2a, the XRD diffraction peaks of MoS_2/G-20 can be accordingly ascribed to the hexagonal phase MoS_2 (JCPDS card No. 77-0341, $R3m$ (160): a = 3.166, b = 3.166, c = 18.410). To further confirm the graphitic nature of carbon layers in the MoS_2/G composite, the inlaid MoS_2 nanoplatelets in MoS_2/G-20 were removed by treating MoS_2/G-20 in concentrated H_2SO_4 solution heated at 120 °C. After heating for 6 h, the precipitate was washed with deionized water and absolute ethanol several times. As shown in the inset of Figure S3, cleaned graphene layers after the removal of inlaid MoS_2 nanoplatelets were be obtained by hot H_2SO_4 treatment. The corresponding XRD pattern and Raman spectrum of cleaned graphene layers revealed relatively high graphitic degree (Figure S3). The EDX spectrum of MoS_2/G-20 (Figure S4) revealed the coexistence of carbon, sulfur, and molybdenum, and the carbon content in the MoS_2/G-20 product was measured to be ∼55.7%, consistent with the TGA (Figure S5) and XPS analysis (Figure S6). The survey spectrum of XPS (Figure S6) was consistent with the above EDX results, and the MoS_2 content in the MoS_2/G-20 product was measured to be ∼37.4 wt %. In the high-resolution XPS spectrum of the C 1s region (Figure 2b), the peak intensity of the C—O and C═O species is very weak, suggesting the successful removal of oxygen-containing groups in molybdenum oleate. The high-resolution XPS spectra of Mo 3d and S 2p regions were investigated to confirm the fabrication of MoS_2 nanoplatelets. The XPS spectrum at the Mo 3d region (Figure 2c) can be deconvoluted into four peaks, and one of these at 226.5 eV corresponds to the S 2s peak of MoS_2. Two characteristic peaks of MoS_2 centered at 229.6 eV (Mo $3d_{5/2}$) and 232.7 eV (Mo $3d_{3/2}$) are observed, while the high binding energy peak at 235.9 eV corresponds to MoO_3 or MoO_4^{2-}, which may result from slight oxidation of the product in air. The sulfur species were determined from the high-resolution XPS spectrum at the S 2p region (Figure 2d). The main doublet centered at binding energies of 161.9 and 163.1 eV corresponds to the S $2p_{3/2}$ and S $2p_{1/2}$ lines of MoS_2, respectively.[41] Meanwhile the binding energies at 164.4 and 168.8 eV can be ascribed to the S_2^{2-} ligands of bridging disulfides and terminal S^{4+} species on the surface or edges of MoS_2 nanoplatelets, respectively.[41,47,48] Raman spectroscopy was used to identify the structure of MoS_2/G-20. As shown in Figure 2e, the intensity ratio of the D band at 1340 cm^{-1} and G band at 1585 cm^{-1} (I_D/I_G) is calculated to be ∼0.77, demonstrating the decent graphitic degree of graphene sheets in the sample. The appearance of the 2D band at about 2670 cm^{-1} further confirmed the formation of graphene sheets. The Raman peaks at about 378.3 and 403.5 cm^{-1} (Figure 2f) are attributed to the in-plane E^1_{2g} and out-of-plane A^1_g vibration modes of Mo−S, respectively.[49,50] In addition, the specific surface area and porous characteristics of the MoS_2/G-20 product were measured by nitrogen adsorption/desorption analysis and pore size distribution measurement. The specific surface area was measured to be 245 m^2/g (Figure S7a) according to the Brunauer−Emmer−Teller (BET) model, and the average pore size based on the Barrett−Joyner−Halenda (BJH) method was ∼5.0 nm (Figure S7b). The high specific surface area and the porous characteristics can facilitate the penetration and permeation of electrolyte ions, thus promoting the HER process.[21]

For comparison, other MoS_2/G-x samples prepared by adding different amounts of Na_2SO_4 crystals were also investigated. As shown in Figure S8, the XRD spectra of MoS_2/G-10, MoS_2/G-15, and MoS_2/G-25 samples show clear diffraction peaks similar to those of MoS_2/G-20, suggesting the

DOI: 10.1021/acs.chemmater.6b01980
Chem. Mater. 2016, 28, 5733−5742

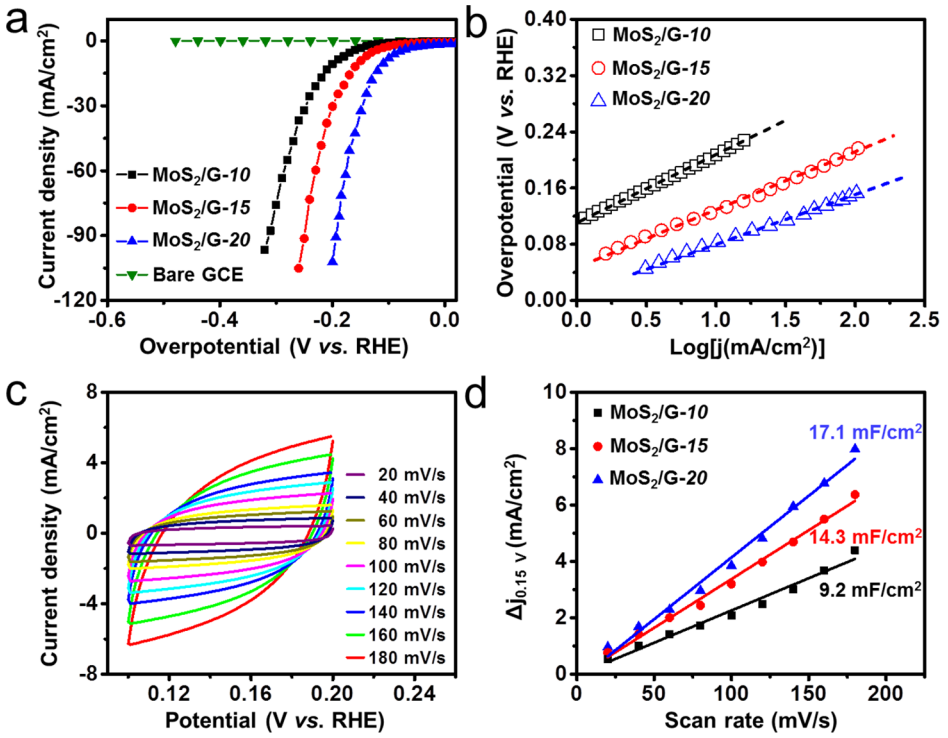

Figure 3. (a) IR-corrected LSV polarization curves of MoS_2/G-10, MoS_2/G-15, and MoS_2/G-20 inlaid nanosheets and bare GCE as HER electrocatalysts. (b) The corresponding Tafel slopes of MoS_2/G-10, MoS_2/G-15, and MoS_2/G-20 inlaid nanosheets. (c) CV curves of MoS_2/G-20 at various scan rates (20−180 mV/s). (d) Capacitive currents at 0.15 V as a function of scan rate for MoS_2/G-10, MoS_2/G-15, and MoS_2/G-20 inlaid nanosheets ($\Delta j_0 = j_a - j_c$).

high consistency and effectiveness of this strategy. The MoS_2 contents in MoS_2/G-10, MoS_2/G-15, and MoS_2/G-25 determined by XPS (Figure S6) were 19.8, 27.8, and 45.1 wt %, respectively. The FESEM and TEM observations of MoS_2/G-10 and MoS_2/G-15 products (Figure S9) revealed the nanostructure similar to that of the MoS_2/G-20 product. However, FESEM characterization (Figure S10) of the MoS_2/G-25 product revealed a very different morphology composed of small nanoparticles and nanoplatelets with amorphous features. The sheet structure of MoS_2/G-25 became fragmented, owing to the partial/incomplete coverage of molybdenum oleate on excessive Na_2SO_4 crystals. In addition, HRTEM images of MoS_2/G-10, MoS_2/G-15, and MoS_2/G-25 products were also provided (Figure S2), and the results demonstrated that the thickness of MoS_2 nanoplates remained stable when the Na_2SO_4 crystal amount increased from 10 to 25 g. The specific surface area and porous characteristics of these MoS_2/G products were also measured. As shown in Figure S11a−f, the specific surface areas of MoS_2/G-10, MoS_2/G-15, and MoS_2/G-25 products were measured to be 104, 182, and 258 m^2/g, respectively, and these samples displayed porous characteristics similar to those of the MoS_2/G-20 product. Thus, the specific surface area of the MoS_2/G-x products increased dramatically with the amount of Na_2SO_4 crystals increased from 10 to 20 g; when the amount of Na_2SO_4 crystals further increased to 25 g, the specific surface area remained almost unchanged. These results suggested that the amount of Na_2SO_4 crystals was critically important for the formation of large-area 2D MoS_2/G inlaid nanosheets with both ultrathin thickness and integral sheet structure, and 20 g of Na_2SO_4 crystals was approaching the limit for obtaining such an intriguing structure.

To further illustrate the structural advantages of MoS_2/G inlaid nanosheets, the MoS_2−graphene composite prepared by a conventional hydrothermal method was also presented as a control sample for comparison. The starting materials included graphene oxide (GO), $Na_2MoO_4{\cdot}2H_2O$, and thiourea. Figure S12 shows the morphology and composition characterizations of the hydrothermally prepared MoS_2−graphene composite. The FESEM images (Figure S12a,b) revealed the typical crumpled and wrinkled structure of the MoS_2−graphene composite. The TEM image (Figure S12c) exhibited the existence of graphene sheets and MoS_2 sheets; the MoS_2 sheets were stacked on graphene sheets, as marked with red arrows. The TEM image with higher magnification (Figure S12d) suggested that no obvious aggregation was observed, indicating the uniform distribution of MoS_2 layers on graphene sheets. Moreover, a typical lamellar structure of MoS_2 with interlayer spacing of 0.63 nm can be observed from the HRTEM image (Figure S12e), and the MoS_2 nanosheets mainly comprise more than five layers. Further XRD characterization (Figure S12f) confirmed the successful preparation of the MoS_2−graphene composite. Compared with this control sample of hydrothermally prepared MoS_2−graphene composites, the MoS_2/G inlaid nanosheets obtained by in situ thermal synthesis displayed smaller and thinner grain sizes of MoS_2 nanoplatelets, as well as much better integration of MoS_2 nanoplatelets and graphene sheets.

The as-prepared large-area 2D MoS_2/G inlaid nanosheets with unique architecture were investigated as the electrocatalysts for HER. Figure 3a shows the *iR*-corrected linear sweep voltammetry (LSV) polarization curves of the MoS_2/G samples within a cathodic potential window of 0 to −0.5 V vs reversible hydrogen electrode (RHE). For comparison, the

DOI: 10.1021/acs.chemmater.6b01980
Chem. Mater. 2016, 28, 5733−5742

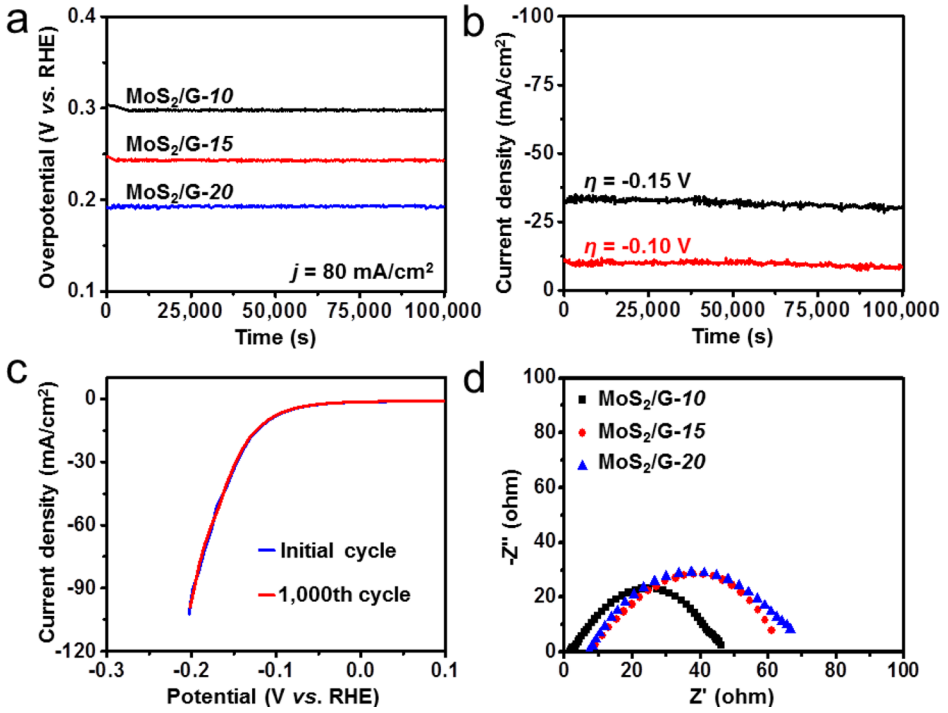

Figure 4. (a) Chronopotentiometric measurements of the long-term stability of MoS_2/G-10, MoS_2/G-15, and MoS_2/G-20 inlaid nanosheets at 80 mA/cm^2. (b) Time-dependent current density curves of MoS_2/G-20 under static overpotential of −0.10 and −0.15 V for 100 000 s. (c) IR-corrected polarization curves of MoS_2/G-20 in 0.50 M H_2SO_4 at the initial cycle and the 1000th cycle of CV scanning between −0.8 and 0.2 V vs RHE. (d) EIS spectra of MoS_2/G-10, MoS_2/G-15, and MoS_2/G-20 samples at η = −0.12 V.

HER catalytic activity of glassy carbon electrode (GCE) is also provided in Figure 3a. Obviously, the GCE alone showed almost no HER catalytic activity; thus, its effect on the electrochemical tests can be certainly neglected. Among the MoS_2/G products, the current densities at the same potential were found to be in the order MoS_2/G-20 > MoS_2/G-15 > MoS_2/G-10, suggesting the highest electrocatalytic activity of the MoS_2/G-20 sample. Strikingly, the MoS_2/G-20 inlaid nanosheets exhibited a low onset overpotential approaching 30 mV and achieved a current density of 10 mA/cm^2 at about 110 mV. In comparison with the control sample of the hydrothermally prepared MoS_2−graphene composite (Figure S12) and other existing MoS_2-based electrocatalysts (Table S1),[32−45] the as-prepared MoS_2/G inlaid nanosheets showed much better HER catalytic activity.

On the basis of the LSV polarization curves of the MoS_2/G samples in Figure 3a, the corresponding Tafel plots were calculated. As shown in Figure 3b, the linear regions of the Tafel plots were well fitted to the Tafel equation ($\eta = b \log j + a$, where b is the Tafel slope and j is the current density). The Tafel slopes of the MoS_2/G-10, MoS_2/G-15, and MoS_2/G-20 electrodes are 96.4, 81.2, and 67.4 mV/dec, respectively. The HER performance of the MoS_2/G-25 product yielded by adding an excessive amount of Na_2SO_4 crystals was also investigated (Figure S13), further suggesting the optimal electrocatalytic activity of MoS_2/G-20 inlaid nanosheets. According to the classical two-electron reaction models, cathodic hydrogen evolution in acidic aqueous media is believed to take place in two steps:[20,51] (1) the "discharge step", in which an electron transfers to a proton at the surface of the electrocatalyst on the cathode, providing an intermediate state of a hydrogen atom bound to an active site (the Volmer reaction: $H^+(aq) + e^- \rightarrow H_{ads}$) and (2) the electrochemical desorption step (the Heyrovsky reaction: $H_{ads} + H^+(aq) + e^- \rightarrow H_2(g)$ or the Tafel recombination reaction: $H_{ads} + H_{ads} \rightarrow H_2(g)$), where H_{ads} represents the H atom absorbed at an active site of electrocatalyst. The Tafel slope is often utilized as an indication of the dominant mechanism, and the rate-determining step in the HER process can be assigned to a Volmer, Heyrovsky, or Tafel reaction by a Tafel slope of 116, 40, or 30 mV/dec, respectively.[52,53] The HER process may occur via the Volmer−Heyrowsky mechanism or the Volmer−Tafel mechanism. However, in both cases, the reaction proceeds through hydrogen atoms adsorbed at the surface of electrocatalyst, and thus the rate of the overall reaction is also influenced by the free energy of hydrogen adsorption, $\Delta G_{H_{ads}}$. The adsorption step would limit the overall reaction rate if the hydrogen to surface bond was too weak, while the reaction−adsorption step would be the dominant step if the hydrogen to surface binding was too strong.[54] According to the density functional theory (DFT) calculations by Hinnemann and co-workers, the hydrogen binding energy of MoS_2 was approximately close to the optimal value of 0 eV.[55] Thus, the obtained Tafel slope of MoS_2/G-20 suggests that the HER on its surface may follow a Heyrovsky dominated Volmer−Heyrovsky mechanism.[56]

Exchange current density (j_0) is one of the most inherent estimations of catalytic activity, which is determined by using the extrapolation method on Tafel plots. The j_0 value of MoS_2/G-20 was measured to be 0.14 mA/cm^2, higher than those of MoS_2/G-15 (0.10 mA/cm^2) and MoS_2/G-10 (0.05 mA/cm^2), implying a much higher catalytic activity. Meanwhile, the exchange current density is usually expressed in terms of ECSA that relates to the number of HER active sites. To estimate the effective surface areas of the MoS_2/G-10, MoS_2/G-15, and MoS_2/G-20 inlaid nanosheets samples, we measured the

DOI: 10.1021/acs.chemmater.6b01980
Chem. Mater. 2016, 28, 5733−5742

electric double layer capacitances (EDLC) at the solid/liquid interfaces of all electrodes by using cyclic voltammetry (CV) measurements with the applied potential in the range of 0.1 to 0.2 V (Figure 3c and Figure S14), where the current response should only be ascribed to the charging/discharging of electric double layers.[57] It is shown (Figure 3d) that the EDLC of MoS_2/G-20 reaches 17.1 mF/cm^2, which is much higher than those of MoS_2/G-15 (14.3 mF/cm^2) and MoS_2/G-10 (9.2 mF/cm^2). Thus, the high exchange current density of MoS_2/G-20 can be associated with its high EDLC. The capacitive performance also indicates that the MoS_2/G-20 sample possesses the highest ECSA for electrochemical reaction, which could certainly contribute to its excellent catalytic activity.[58,59] In this work, Na_2SO_4 crystals served as the template for the formation of 2D MoS_2/G inlaid nanosheets. As the amount of Na_2SO_4 crystals increased from 10 to 20 g, the specific surface area of the MoS_2/G-x samples greatly increased for 104 m^2/g to 245 m^2/g (Figures S7 and S11), and thus the number of active sites also increased accordingly. Furthermore, the EDLC and ECSA of MoS_2/G inlaid nanosheets were also increased along with the amount of Na_2SO_4 crystals (Figure 3d). These results are consistent with the above BET analysis. Therefore, it indicates that the key reason for dramatic difference in the catalytic activity among MoS_2/G-10, MoS_2/G-15, and MoS_2/G-20 should be the number of exposed active sites for HER.

The estimation of turnover frequency (TOF) makes it possible to compare the catalytic activity of MoS_2/G-20 with other reported HER catalysts. The number of the active sites was quantified by the electrochemical method.[60] Figure S15a shows the CV curve of MoS_2/G-20 at 50 mV s^{-1} in the phosphate buffered saline (PBS, pH = 7.0) solution. Assuming a one-electron process for both reduction and oxidation, the upper limit of the active sites could be calculated. Figure S15b displays the polarization curve normalized by the active sites and expressed in terms of TOF. The overpotentials of MoS_2/G-20 electrocatalyst with the TOF values of 4.0 and 7.0 s^{-1} were 110 and 130 mV, respectively. Compared to other reported HER catalysts,[61,62] MoS_2/G-20 exhibits much higher TOF values under the same overpotentials, suggesting the higher electrocatalytic activity toward HER. In addition, the Faradaic efficiency of MoS_2/G-20 was probed by comparing the volume of generated gas and the quantity of charges passed the MoS_2/G-20 electrode in a potentiostatic electrolysis measurement carried out at an overpotential of −0.15 V for 1540 s. As shown in Figure S16, the Faradaic efficiency of MoS_2/G-20 for HER was close to 100%.

Electrochemical stability is another important criterion for a good electrocatalyst. To evaluate the stability of the as-synthesized MoS_2/G electrocatalysts, long-duration chronopotentiometric measurements of HER were conducted at a current density of 80 mA/cm^2, as shown in Figure 4a. The overpotentials of the MoS_2/G-10, MoS_2/G-15, and MoS_2/G-20 inlaid nanosheets samples remained almost unchanged for 100 000 s, implying the ultrahigh stability of these electrocatalysts. Impressively, the MoS_2/G-20 sample still shows a small overpotential of around −0.19 V after HER testing for 100 000 s, which was much lower than those of MoS_2/G-15 (−0.24 V) and MoS_2/G-10 (−0.30 V) under the same condition. Figure 4b presents the time-dependent current density curves of MoS_2/G-20 under static overpotentials (η) of −0.10 and −0.15 V, respectively. After a long HER testing period (100 000 s), the current densities only showed slight degradation (with ∼97% of activity retention under η = −0.15 V), which could be owing to the consumption of protons in the reaction system and the hindrance of reaction by hydrogen bubbles remaining on the catalyst.[54] To further demonstrate the high electrochemical stability intuitively, we measured the LSV polarization curves at the initial cycle and after 1000 cycles of CV scanning. As shown in Figure 4c, at the 1000th cycle, the polarization curve of MoS_2/G-20 exhibited negligible difference as compared with the initial one. In addition, the electrochemical impedance spectroscopy (EIS) spectra of MoS_2/G products were investigated at η = −0.12 V, as shown in Figure 4d. The resistance of the MoS_2/G-20 product was measured to be ∼60 Ω, much smaller than those of other MoS_2/graphene composites.[43,63] It proves that the underlying graphene sheets afforded smooth electron transfer from the less-conductive MoS_2 to the electrode, which is one of the key factors contributing to the superior kinetics toward HER. In sharp contrast, the control sample of the hydrothermally prepared MoS_2−graphene composite revealed a poor electrocatalytic activity and much inferior cycle stability for the first 40 000 s (Figure S17). This result is undoubtedly attributed to the structural difference between MoS_2/G inlaid nanosheets and MoS_2−graphene composite. Compared to MoS_2/G inlaid nanosheets, the conventional MoS_2−graphene composite exhibited a smaller number of exposed active sites and weaker interaction between MoS_2 and graphene sheets. To further confirm the excellent stability of the MoS_2/G inlaid nanosheets, the morphology of MoS_2/G-20 after long-term stability tests was investigated. As shown in Figure S18, the structure of MoS_2/G-20 was perfectly retained after HER testing for 100 000 s, suggesting the extraordinary structural stability as compared to other MoS_2 based electrocatalysts (Table S1).[32−45]

The excellent HER performance of the MoS_2/G inlaid nanosheets can be attributed to its unique architecture, which features the following advantages: (1) The ultrathin MoS_2 nanoplatelets homogeneously inlaid in graphene nanosheets provided a huge number of exposed active sites, thus significantly promoting the HER process.[64,65] (2) The as-formed graphene sheets served dual functions as the conductive channels for accelerating the electron transfer and also as the trapping agent for absorbing H^+ ions.[66] (3) The strong bonding and remarkable coordination of MoS_2 and graphene ensured the high structural stability of MoS_2/G inlaid nanosheets in long-term electrochemical measurements. All of these factors are beneficial to the enhancement of HER performance. This is the reason why the MoS_2/graphene inlaid nanosheets present ultrahigh catalytic activity toward HER and outstanding long-term electrochemical stability that cannot be obtained by other electrocatalysts with similar compositions.

■ CONCLUSIONS

In summary, we have rationally designed and fabricated a novel 2D hybrid architecture consisting of ultrathin MoS_2 nanoplatelets inlaid in graphene sheets via a unique thermal synthesis strategy. Electrochemical measurements revealed that the MoS_2/G inlaid nanosheets exhibited ultrahigh catalytic activity toward HER and excellent electrochemical stability after long-duration testing in acidic solution. It proves that the large amount of exposed active sites on MoS_2 nanoplatelets and excellent electrical conductivity of graphene sheets synergistically contributed to the ultrahigh electrocatalytic performance. In addition to the MoS_2 or graphene based electrocatalysts, the

DOI: 10.1021/acs.chemmater.6b01980
Chem. Mater. 2016, 28, 5733−5742

effective and universal strategy used in this work paves the way to synthesize other 2D inlaid nanostructures with diverse potential applications.

■ ASSOCIATED CONTENT

Supporting Information

The Supporting Information is available free of charge on the ACS Publications website at DOI: 10.1021/acs.chemmater.6b01980.

Table S1, calibration of SCE, calculation of active sites and TOF, and Figures S1−S18 (PDF)

■ AUTHOR INFORMATION

Corresponding Authors

*E-mail: zhongjin@nju.edu.cn (Z. Jin).
*E-mail: j.liu@duke.edu (J. Liu).

Notes

The authors declare no competing financial interest.

■ ACKNOWLEDGMENTS

This work is supported by the National Thousand Young Talents Program of China, the Young Scientists Project of National Basic Research Program of China (973 Program No. 2015CB659300), the National Natural Science Foundation of China (NSFC Grant No. 21403105 and No. 21573108), the China Postdoctoral Science Foundation (Grant No. 2015M580408, No. 2015M580413, and No. 2015M581769), the Natural Science Foundation for Young Scholars of Jiangsu Province (Grant No. BK20150571 and No. BK20150583), the Fundamental Research Funds for the Central Universities, and a project funded by the Priority Academic Program Development of Jiangsu Higher Education Institutions (PAPD).

■ REFERENCES

(1) Cortright, R. D.; Davda, R. R.; Dumesic, J. A. Hydrogen from Catalytic Reforming of Biomass-derived Hydrocarbons in Liquid Water. *Nature* **2002**, *418*, 964−967.

(2) Faber, M. S.; Jin, S. Earth-abundant Inorganic Electrocatalysts and Their Nanostructures for Energy Conversion Applications. *Energy Environ. Sci.* **2014**, *7*, 3519−3542.

(3) Lewis, N. S.; Nocera, D. G. Powering the Planet: Chemical Challenges in Solar Energy Utilization. *Proc. Natl. Acad. Sci. U. S. A.* **2006**, *103*, 15729−15735.

(4) Gratzel, M. Recent Advances in Sensitized Mesoscopic Solar Cells. *Acc. Chem. Res.* **2009**, *42*, 1788−1798.

(5) Dresselhaus, M. S.; Thomas, I. L. Alternative Energy Technologies. *Nature* **2001**, *414*, 332−337.

(6) Turner, J. A. Sustainable Hydrogen Production. *Science* **2004**, *305*, 972−974.

(7) Chen, W. F.; Iyer, S.; Iyer, S.; Sasaki, K.; Wang, C. H.; Zhu, Y. M.; Muckerman, J. T.; Fujita, E. Biomass-derived Electrocatalytic Composites for Hydrogen Evolution. *Energy Environ. Sci.* **2013**, *6*, 1818−1826.

(8) Chen, Z. F.; Ye, S. R.; Wilson, A. R.; Ha, Y. C.; Wiley, B. J. Optically Transparent Hydrogen Evolution Catalysts Made from Networks of Copper−Platinum Core−shell Nanowires. *Energy Environ. Sci.* **2014**, *7*, 1461−1467.

(9) Lu, Z. Y.; Zhang, H. C.; Zhu, W.; Yu, X. Y.; Kuang, Y.; Chang, Z.; Lei, X. D.; Sun, X. M. *In Situ* Fabrication of Porous MoS_2 Thin-Films as High-performance Catalysts for Electrochemical Hydrogen Evolution. *Chem. Commun.* **2013**, *49*, 7516−7518.

(10) Ma, L. B.; Shen, X. P.; Zhu, J.; Zhu, G. X.; Ji, Z. Y. Co_3ZnC Core−shell Nanoparticle Assembled Microspheres/Reduced Graphene Oxide as An Advanced Electrocatalyst for Hydrogen Evolution Reaction in An Acidic Solution. *J. Mater. Chem. A* **2015**, *3*, 11066−11073.

(11) Gray, H. B. Powering the Planet with Solar Fuel. *Nat. Chem.* **2009**, *1*, 7−7.

(12) Millet, P.; Andolfatto, F.; Durand, R. Design and Performance of A Solid Polymer Electrolyte Water Electrolyzer. *Int. J. Hydrogen Energy* **1996**, *21*, 87−93.

(13) Jia, L. P.; Sun, X.; Jiang, Y. M.; Yu, S. J.; Wang, C. M. Novel $MoSe_2$−Reduced Graphene Oxide/Polyimide Composite Film for Applications in Electrocatalysis and Photoelectrocatalysis Hydrogen Evolution. *Adv. Funct. Mater.* **2015**, *25*, 1814−1820.

(14) Jaramillo, T. F.; Jorgensen, K. P.; Bonde, J.; Nielsen, J. H.; Horch, S.; Chorkendorff, I. Identification of Active Edge Sites for Electrochemical H_2 Evolution from MoS_2 Nanocatalysts. *Science* **2007**, *317*, 100−102.

(15) Gao, M. R.; Lin, Z. Y.; Zhuang, T. T.; Jiang, J.; Xu, Y. F.; Zheng, Y. R.; Yu, S. H. Mixed-solution Synthesis of Sea Urchin-like NiSe Nanofiber Assemblies as Economical Pt-Free Catalysts for Electrochemical H_2 Production. *J. Mater. Chem.* **2012**, *22*, 13662−13668.

(16) Tang, H.; Dou, K. P.; Kaun, C. C.; Kuang, Q.; Yang, S. H. $MoSe_2$ Nanosheets and Their Graphene Hybrids: Synthesis, Characterization and Hydrogen Evolution Reaction Studies. *J. Mater. Chem. A* **2014**, *2*, 360−364.

(17) Shi, Y. M.; Xu, Y.; Zhuo, S. F.; Zhang, J. F.; Zhang, B. Ni_2P Nanosheets/Ni Foam Composite Electrode for Long-Lived and pH-Tolerable Electrochemical Hydrogen Generation. *ACS Appl. Mater. Interfaces* **2015**, *7*, 2376−2384.

(18) Xing, Z.; Liu, Q.; Asiri, A. M.; Sun, X. P. High-Efficiency Electrochemical Hydrogen Evolution Catalyzed by Tungsten Phosphide Submicroparticles. *ACS Catal.* **2015**, *5*, 145−149.

(19) Callejas, J. F.; McEnaney, J. M.; Read, C. G.; Crompton, J. C.; Biacchi, A. J.; Popczun, E. J.; Gordon, T. R.; Lewis, N. S.; Schaak, R. E. Electrocatalytic and Photocatalytic Hydrogen Production from Acidic and Neutral-pH Aqueous Solutions Using Iron Phosphide Nanoparticles. *ACS Nano* **2014**, *8*, 11101−11107.

(20) Huang, Z. P.; Chen, Z. B.; Chen, Z. Z.; Lv, C. C.; Meng, H.; Zhang, C. $Ni_{12}P_5$ Nanoparticles as an Efficient Catalyst for Hydrogen Generation *via*Electrolysis and Photoelectrolysis. *ACS Nano* **2014**, *8*, 8121−8129.

(21) Xing, Z.; Liu, Q.; Asiri, A. M.; Sun, X. P. Closely Interconnected Network of Molybdenum Phosphide Nanoparticles: A Highly Efficient Electrocatalyst for Generating Hydrogen from Water. *Adv. Mater.* **2014**, *26*, 5702−5707.

(22) Chen, W. F.; Sasaki, K.; Ma, C.; Frenkel, A. I.; Marinkovic, N.; Muckerman, J. T.; Zhu, Y. M.; Adzic, R. R. Hydrogen-Evolution Catalysts Based on Non-Noble Metal Nickel− Molybdenum Nitride Nanosheets. *Angew. Chem., Int. Ed.* **2012**, *51*, 6131−6135.

(23) Chen, W.-F.; Iyer, S.; Iyer, S.; Sasaki, K.; Wang, C.-H.; Zhu, Y.; Muckerman, J. T.; Fujita, E. Biomass-derived Electrocatalytic Composites for Hydrogen Evolution. *Energy Environ. Sci.* **2013**, *6*, 1818−1826.

(24) Choi, D.; Kumta, P. N. Synthesis, Structure, and Electrochemical Characterization of Nanocrystalline Tantalum and Tungsten Nitrides. *J. Am. Ceram. Soc.* **2007**, *90*, 3113−3120.

(25) Cao, B. F.; Veith, G. M.; Neuefeind, J. C.; Adzic, R. R.; Khalifah, P. G. Mixed Close-Packed Cobalt Molybdenum Nitrides as Non-noble Metal Electrocatalysts for the Hydrogen Evolution Reaction. *J. Am. Chem. Soc.* **2013**, *135*, 19186−19192.

(26) Harnisch, F.; Sievers, G.; Schroder, U. Tungsten Carbide as Electrocatalyst for the Hydrogen Evolution Reaction in pH Neutral Electrolyte Solutions. *Appl. Catal., B* **2009**, *89*, 455−458.

(27) Esposito, D. V.; Hunt, S. T.; Stottlemyer, A. L.; Dobson, K. D.; McCandless, B. E.; Birkmire, R. W.; Chen, J. G. G. Low-Cost Hydrogen-Evolution Catalysts Based on Monolayer Platinum on Tungsten Monocarbide Substrates. *Angew. Chem., Int. Ed.* **2010**, *49*, 9859−9862.

(28) Weidman, M. C.; Esposito, D. V.; Hsu, Y.-C.; Chen, J. G. Comparison of Electrochemical Stability of Transition Metal Carbides

DOI: 10.1021/acs.chemmater.6b01980
Chem. Mater. 2016, 28, 5733−5742

(WC, W_2C, Mo_2C) over A Wide pH Range. *J. Power Sources* **2012**, *202*, 11−17.
(29) Ham, D. J.; Ganesan, R.; Lee, J. S. Tungsten Carbide Microsphere as An Electrode for Cathodic Hydrogen Evolution from Water. *Int. J. Hydrogen Energy* **2008**, *33*, 6865−6873.
(30) Chhowalla, M.; Shin, H. S.; Eda, G.; Li, L. J.; Loh, K. P.; Zhang, H. The Chemistry of Two-dimensional Layered Transition Metal Dichalcogenide Nanosheets. *Nat. Chem.* **2013**, *5*, 263−275.
(31) Laursen, A. B.; Kegnaes, S.; Dahl, S.; Chorkendorff, I. Molybdenum Sulfides—Efficient and Viable Materials for Electro- and Photoelectrocatalytic Hydrogen Evolution. *Energy Environ. Sci.* **2012**, *5*, 5577−5591.
(32) Chung, D. Y.; Park, S. K.; Chung, Y. H.; Yu, S. H.; Lim, D. H.; Jung, N.; Ham, H. C.; Park, H. Y.; Piao, Y.; Yoo, S. J.; Sung, Y. E. Edge-exposed MoS_2 nano-assembled structures as efficient electrocatalysts for hydrogen evolution reaction. *Nanoscale* **2014**, *6*, 2131−2136.
(33) Ye, T. N.; Lv, L. B.; Xu, M.; Zhang, B.; Wang, K. X.; Su, J.; Li, X. H.; Chen, J. S. Hierarchical Carbon Nanopapers Coupled with Ultrathin MoS_2 Nanosheets: Highly Efficient Large-area Electrodes for Hydrogen Evolution. *Nano Energy* **2015**, *15*, 335−342.
(34) Zhou, W. J.; Zhou, K.; Hou, D. M.; Liu, X. J.; Li, G. Q.; Sang, Y. H.; Liu, H.; Li, L. G.; Chen, S. W. MoS_2 Nanocube Structures as Catalysts for Electrochemical H_2 Evolution from Acidic Aqueous Solutions. *ACS Appl. Mater. Interfaces* **2014**, *6*, 21534−21540.
(35) Shi, J. P.; Ma, D. L.; Han, G. F.; Zhang, Y.; Ji, Q. Q.; Gao, T.; Sun, J. Y.; Song, X. J.; Li, C.; Zhang, Y. S.; Lang, X. Y.; Zhang, Y. F.; Liu, Z. F. Controllable Growth and Transfer of Monolayer MoS_2 on Au Foils and Its Potential Application in Hydrogen Evolution Reaction. *ACS Nano* **2014**, *8*, 10196−10204.
(36) Geng, X. M.; Wu, W.; Li, N.; Sun, W. W.; Armstrong, J.; Al-hilo, A.; Brozak, M.; Cui, J. B.; Chen, T. P. Three-Dimensional Structures of MoS_2Nanosheets with Ultrahigh Hydrogen Evolution Reaction in Water Reduction. *Adv. Funct. Mater.* **2014**, *24*, 6123−6129.
(37) Yang, Y.; Fei, H. L.; Ruan, G. D.; Xiang, C. S.; Tour, J. M. Edge-oriented MoS_2 Nanoporous Films as Flexible Electrodes for Hydrogen Evolution Reactions and Supercapacitor devices. *Adv. Mater.* **2014**, *26*, 8163−8168.
(38) Firmiano, E. G. S.; Cordeiro, M. A. L.; Rabelo, A. C.; Dalmaschio, C. J.; Pinheiro, A. N.; Pereira, E. C.; Leite, E. R. Graphene Oxide as A Highly Selective Substrate to Synthesize a Layered MoS_2 Hybrid Electrocatalyst. *Chem. Commun.* **2012**, *48*, 7687−7689.
(39) Zhu, H.; Du, M. L.; Zhang, M.; Zou, M. L.; Yang, T. T.; Wang, S. L.; Yao, J. M.; Guo, B. C. S-rich Single-layered MoS_2 Nanoplates Embedded in N-doped Carbon Nanofibers: Efficient Co-electrocatalysts for the Hydrogen Evolution Reaction. *Chem. Commun.* **2014**, *50*, 15435−15438.
(40) Wang, T. Y.; Gao, D. L.; Zhuo, J. Q.; Zhu, Z. W.; Papakonstantinou, P.; Li, Y.; Li, M. X. Size-Dependent Enhancement of Electrocatalytic Oxygen-Reduction and Hydrogen-Evolution Performance of MoS_2 Particles. *Chem. - Eur. J.* **2013**, *19*, 11939−11948.
(41) Zheng, X. L.; Xu, J. B.; Yan, K. Y.; Wang, H.; Wang, Z. L.; Yang, S. H. Space-Confined Growth of MoS_2 Nanosheets within Graphite: The Layered Hybrid of MoS_2 and Graphene as an Active Catalyst for Hydrogen Evolution Reaction. *Chem. Mater.* **2014**, *26*, 2344−2353.
(42) Yan, Y.; Xia, B. Y.; Li, N.; Xu, Z. C.; Fisher, A.; Wang, X. Vertically Oriented MoS_2 and WS_2 Nanosheets Directly Grown on Carbon Cloth as Efficient and Stable 3-Dimensional Hydrogen-Evolving Cathodes. *J. Mater. Chem. A* **2015**, *3*, 131−135.
(43) Li, Y. G.; Wang, H. L.; Xie, L. M.; Liang, Y. Y.; Hong, G. S.; Dai, H. J. MoS_2 Nanoparticles Grown on Graphene: An Advanced Catalyst for the Hydrogen Evolution Reaction. *J. Am. Chem. Soc.* **2011**, *133*, 7296−7299.
(44) Ma, C. B.; Qi, X. Y.; Chen, B.; Bao, S. Y.; Yin, Z. Y.; Wu, X. J.; Luo, Z. M.; Wei, J.; Zhang, H. L.; Zhang, H. MoS_2 Nanoflower-Decorated Reduced Graphene Oxide Paper for High-Performance Hydrogen Evolution Reaction. *Nanoscale* **2014**, *6*, 5624−5629.
(45) Yan, Y.; Ge, X. M.; Liu, Z. L.; Wang, J. Y.; Lee, J. M.; Wang, X. Facile Synthesis of Low Crystalline MoS_2 Nanosheet-Coated CNTs for Enhanced Hydrogen Evolution Reaction. *Nanoscale* **2013**, *5*, 7768−7771.
(46) Hummers, W. S.; Offeman, R. E. Preparation of Graphitic Oxide. *J. Am. Chem. Soc.* **1958**, *80*, 1339−1339.
(47) Wang, T. Y.; Liu, L.; Zhu, Z. W.; Papakonstantinou, P.; Hu, J. B.; Liu, H. Y.; Li, M. X. Enhanced Electrocatalytic Activity for Hydrogen Evolution Reaction from Self-assembled Monodispersed Molybdenum Sulfide Nanoparticles on An Au Electrode. *Energy Environ. Sci.* **2013**, *6*, 625−633.
(48) Li, F.; Zhang, L.; Li, J.; Lin, X. Q.; Li, X. Z.; Fang, Y. Y.; Huang, J. W.; Li, W. Z.; Tian, M.; Jin, J.; Li, R. Synthesis of Cu-MoS_2/rGO Hybrid as Non-Noble Metal Electrocatalysts for the Hydrogen Evolution Reaction. *J. Power Sources* **2015**, *292*, 15−22.
(49) Zhu, H.; Lyu, F. L.; Du, M. L.; Zhang, M.; Wang, Q. F.; Yao, J. M.; Guo, B. C. Design of Two-Dimensional, Ultrathin MoS_2 Nanoplates Fabricated Within One-Dimensional Carbon Nanofibers With Thermosensitive Morphology: High-Performance Electrocatalysts For The Hydrogen Evolution Reaction. *ACS Appl. Mater. Interfaces* **2014**, *6*, 22126−22137.
(50) Liu, N.; Yang, L. C.; Wang, S. N.; Zhong, Z. W.; He, S. N.; Yang, X. Y.; Gao, Q. S.; Tang, Y. Ultrathin MoS_2 Nanosheets Growing within An *In-Situ*-Formed Template as Efficient Electrocatalysts for Hydrogen Evolution. *J. Power Sources* **2015**, *275*, 588−594.
(51) Durst, J.; Siebel, A.; Simon, C.; Hasche, F.; Herranz, J.; Gasteiger, H. A. New Insights into the Electrochemical Hydrogen Oxidation and Evolution Reaction Mechanism. *Energy Environ. Sci.* **2014**, *7*, 2255−2260.
(52) Chen, W. F.; Muckerman, J. T.; Fujita, E. Recent Developments in Transition Metal Carbides and Nitrides as Hydrogen Evolution Electrocatalysts. *Chem. Commun.* **2013**, *49*, 8896−8909.
(53) Ma, L. B.; Shen, X. P.; Zhou, H.; Zhu, G. X.; Ji, Z. Y.; Chen, K. M. CoP Nanoparticles Deposited on Reduced Graphene Oxide Sheets as An Active Electrocatalyst for The Hydrogen Evolution Reaction. *J. Mater. Chem. A* **2015**, *3*, 5337−5343.
(54) Benck, J. D.; Hellstern, T. R.; Kibsgaard, J.; Chakthranont, P.; Jaramillo, T. F. Catalyzing the Hydrogen Evolution Reaction (HER) with Molybdenum Sulfide Nanomaterials. *ACS Catal.* **2014**, *4*, 3957−3971.
(55) Hinnemann, B.; Moses, P. G.; Bonde, J.; Jorgensen, K. P.; Nielsen, J. H.; Horch, S.; Chorkendorff, I.; Norskov, J. K. Biomimetic Hydrogen Evolution: MoS_2 Nanoparticles as Catalyst for Hydrogen Evolution. *J. Am. Chem. Soc.* **2005**, *127*, 5308−5309.
(56) Zhu, Y. P.; Xu, X. Y.; Su, H.; Liu, Y. P.; Chen, T. H.; Yuan, Z. Y. Ultrafine Metal Phosphide Nanocrystals *in Situ* Decorated on Highly Porous Heteroatom-Doped Carbons for Active Electrocatalytic Hydrogen Evolution. *ACS Appl. Mater. Interfaces* **2015**, *7*, 28369−28376.
(57) Fan, X. J.; Peng, Z. W.; Ye, R. Q.; Zhou, H. Q.; Guo, X. M_3C (M: Fe, Co, Ni) Nanocrystals Encased in Graphene Nanoribbons: An Active and Stable Bifunctional Electrocatalyst for Oxygen Reduction and Hydrogen Evolution Reactions. *ACS Nano* **2015**, *9*, 7407−7418.
(58) Tian, J. Q.; Liu, Q.; Cheng, N. Y.; Asiri, A. M.; Sun, X. P. Self-Supported Cu3P Nanowire Arrays as An Integrated High-Performance Three-Dimensional Cathode for Generating Hydrogen from Water. *Angew. Chem., Int. Ed.* **2014**, *53*, 9577−9581.
(59) Kong, D.; Wang, H.; Lu, Z.; Cui, Y. $CoSe_2$ Nanoparticles Grown on Carbon Fiber Paper: An Efficient and Stable Electrocatalyst for Hydrogen Evolution Reaction. *J. Am. Chem. Soc.* **2014**, *136*, 4897−4900.
(60) Merki, D.; Fierro, S.; Vrubel, H.; Hu, X. Amorphous Molybdenum Sulfide Films as Catalysts for Electrochemical Hydrogen Production in Water. *Chem. Sci.* **2011**, *2*, 1262−1267.
(61) Chen, Z. B.; Cummins, D.; Reinecke, B. N.; Clark, E.; Sunkara, M. K.; Jaramillo, T. F. Core−shell MoO_3−MoS_2 Nanowires for Hydrogen Evolution: A Functional Design for Electrocatalytic Materials. *Nano Lett.* **2011**, *11*, 4168−4175.

DOI: 10.1021/acs.chemmater.6b01980
Chem. Mater. 2016, 28, 5733−5742

(62) Xiao, P.; Chen, W.; Wang, X. A Review of Phosphide-Based Materials for Electrocatalytic Hydrogen Evoution. *Adv. Energy Mater.* **2015**, *5*, 1500985.
(63) Liao, L.; Zhu, J.; Bian, X. J.; Zhu, L. N.; Scanlon, M. D.; Girault, H. H.; Liu, B. H. MoS_2 Formed on Mesoporous Graphene as A Highly Active Catalyst for Hydrogen Evolution. *Adv. Funct. Mater.* **2013**, *23*, 5326−5333.
(64) Yu, Y. F.; Huang, S. Y.; Li, Y. P.; Steinmann, S. N.; Yang, W. T.; Cao, L. Layer-Dependent Electrocatalysis of MoS_2 for Hydrogen Evolution. *Nano Lett.* **2014**, *14*, 553−558.
(65) Lu, Z. Y.; Zhang, H. C.; Zhu, W.; Yu, X. Y.; Kuang, Y.; Chang, Z.; Lei, X. D.; Sun, X. M. *In Situ* Fabrication of Porous MoS_2 Thin-Films as High-Performance Catalysts for Electrochemical Hydrogen Evolution. *Chem. Commun.* **2013**, *49*, 7516−7518.
(66) Lu, Z.; Chang, Z.; Zhu, W.; Sun, X. Beta-phased $Ni(OH)_2$ Nanowall Film with Reversible Capacitance Higher Than Theoretical Faradic Capacitance. *Chem. Commun.* **2011**, *47*, 9651−9653.

DOI: 10.1021/acs.chemmater.6b01980
Chem. Mater. 2016, 28, 5733−5742